A New Parameter Estimation Method for DSC Thermodynamic Property Evaluation – Part II: Runge–Kutta Implementation and Numerical Results

G. E. Osborne, Ph.D. Candidate
J. I. Frankel, Professor
Mechanical and Aerospace Engineering and Engineering Science Department
University of Tennessee
Knoxville, Tennessee (USA) 37996-2210
email: gosborne@utk.edu
A. S. Sabau, Research Staff Member
Oak Ridge National Laboratory
1 Bethel Valley Road
Oak Ridge, Tennessee (USA) 37831-6083

ABSTRACT
A lumped heat transfer model and parameter estimation technique are proposed for determining key parameters associated with a heat flux *Differential Scanning Calorimeter* (DSC). The development of a mathematical algorithm utilizing this model and technique is illustrated in Part I of this two-part paper. In Part II, a computational algorithm which has been constructed for the proposed method is presented. The algorithm uses a conventional fourth-order Runge-Kutta scheme to solve the necessary ordinary differential equations. Results from a numerical experiment are discussed. These results demonstrate the robust and accurate nature of the technique but also suggest areas of possible improvement for both computational efficiency and parameter resolution. Possible improvements include the introduction of an elliptic time treatment in the form of orthogonal collocation as a replacement for the traditional time-marching scheme.

KEY WORDS
Parameter estimation, inverse problems, Function Decomposition Method, DSC

1 Introduction

This paper presents numerical results using the algorithm outlined in the companion article [1]. The goal of this study involves developing a practical inverse technique that can be applied to enhance conventional DSC analysis. The methodology described in [1] is presently tested for reconstruction accuracy and stability. It is interesting to note that the proposed methodology encompasses elements from both parameter estimation and function reconstruction.

To begin, a direct problem is defined in which the system parameters K_{sp}, K_{rp}, E_{fp}, E_{fc}, and forcing function $T_f(t)$ are specified. The outcomes from the direct analysis lead to converged numerical results for $T_s(t)$, $T_r(t)$, $T_{rp}(t)$ and $T_{sp}(t)$. Next, noise is added to the direct solution for $T_{rp}(t)$ and $T_{sp}(t)$. These newly constructed data sets now represent the input to the inverse problem. This paper begins by describing the test problem from which data are numerically simulated for the sample and reference plates. Once these data are obtained, numerical testing of the inverse method can be considered with the goal of recapturing the system parameters and the furnace wall temperature associated with defining the direct problem.

Before delving into the numerics, a sidebar is offered with regard to the mathematical model under consideration. It should be observed from the proposed reduced physical model [1] that no inter-radiative coupling exists between the sample and reference sides. Radiative heating from the furnace wall is the driver to both regions. Additionally, all conductive communication is solely between each plate-container region. This lack of cross communication between the reference and sample necessitates the use of a two-concurrent data stream model. The ultimate goal is to develop a method that can reconstruct the furnace temperature and system heat transfer parameters. It should also be noted that most, if not all, previous studies assume a priori knowledge of the furnace wall temperature. A pure parameter estimation study results once this function is assumed known. Many DSC's have LED readouts that provide the user with some indication of the furnace temperature. This readout, however, may not truly represent the furnace $wall$ temperature, $T_f(t)$.

2 Solution of the Direct Problem

In order to illustrate the robust nature of the analytical model presented in the first part of this paper [1], a direct problem has been formulated to provide computationally

generated temperature data for both the sample and reference plates. Naturally, this direct problem is based upon the same simplified model and governing equations used to develop the inverse parameter estimation algorithm, that is,

$$\alpha_s \frac{dT_s}{dt} = K_{sp}(T_{sp} - T_s) + E_{fc}(T_f^4 - T_s^4), \quad (1a)$$

$$\alpha_r \frac{dT_r}{dt} = K_{rp}(T_{rp} - T_r) + E_{fc}(T_f^4 - T_r^4), \quad (1b)$$

$$\alpha_{sp} \frac{dT_{sp}}{dt} = -K_{sp}(T_{sp} - T_s) + E_{fp}(T_f^4 - T_{sp}^4), \quad (1c)$$

$$\alpha_{rp} \frac{dT_{rp}}{dt} = -K_{rp}(T_{rp} - T_r) + E_{fp}(T_f^4 - T_{rp}^4), \quad t \geq 0, \quad (1d)$$

with the initial conditions

$$T_s(0) = T_{sp}(0) = T_r(0) = T_{rp}(0) = T_o. \quad (1e)$$

In this case, the parameters K_{sp}, K_{rp}, E_{fc}, and E_{fp} are assumed to be known and, as a first approximation, independent of temperature.

Unlike with the more difficult inverse problem, the furnace wall temperature, T_f, is assumed to be a known function in the direct problem and so provides the forcing mechanism for the system. As a result, the governing equations for the sample and sample plate temperatures are decoupled from the equations for the reference and reference plate temperatures, producing two systems of two coupled equations each. These systems of nonlinear ordinary differential equations may be easily solved using a fourth–order Runge–Kutta scheme.

It is reasonable to assume that the furnace response to a change in applied heating or cooling rate is rapid and that the rate is maintained as constant throughout the heating or cooling process. A temperature profile based on these assumptions is shown in Figure 1. The time interval $0 \leq t < t_0$ represents a short amount of the isothermal heating period used to establish initial conditions for the DSC elements. For the interval $t_0 \leq t < t_2$, heating at a constant rate occurs. Likewise, for the interval $t_2 \leq t \leq t_{max}$, cooling at the same constant rate occurs. A small response lag has been included near the times of transition to heating or cooling to provide a more realistic temperature profile. Based on this representation of furnace wall temperature, the following driving function can be constructed

$$T_f(t) = T_o, \qquad t \in [0, t_0], \quad (2a)$$

$$T_f(t) = T_o + \mu\left(1 - e^{-\beta\tau}\right)\tau, \qquad t \in [t_0, t_1], \quad (2b)$$

$$T_f(t) = T_{max} - \mu\left(1 - e^{-\beta(\tau_2 - \tau)}\right)(\tau_2 - \tau), \qquad t \in [t_1, t_2], \quad (2c)$$

$$T_f(t) = T_{max} - \mu\left(1 - e^{-\beta(\tau - \tau_2)}\right)(\tau - \tau_2), \qquad t \in [t_2, t_{max}], \quad (2d)$$

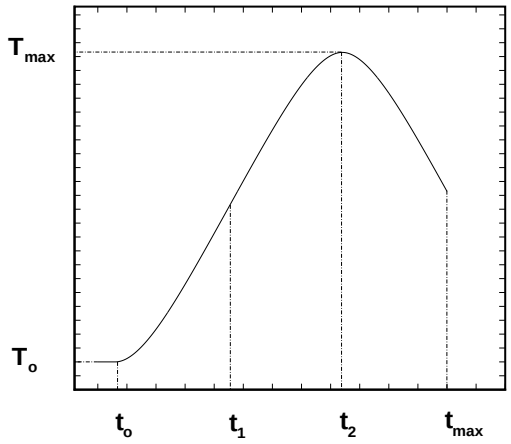

Figure 1. Generic furnace wall temperature profile used as the driving function for the direct problem.

where

$$\tau = t - t_0. \quad (2e)$$

Additionally, μ is the heating rate in Kelvins per second, and β is a coefficient which is proportional to the furnace response time. In order to maintain continuity in both temperature and heating rate, t_1 is chosen such that

$$t_1 = t_0 + \frac{t_2 - t_0}{2}, \quad (3a)$$

yielding the expression for maximum attained furnace temperature as

$$T_{max} = T_o + 2\mu\left(1 - e^{-\beta\tau_1}\right)\tau_1. \quad (3b)$$

The model for the direct problem as described above is stable and produces accurate and reliable temperature data for use in the parameter estimation algorithm.

3 Computational Algorithm for the Parameter Estimation Problem

An optimized computational algorithm, written in ANSI Standard Fortran, has been developed based on the mathematical model introduced in the first part of this paper [1]. The basic logic for this algorithm is illustrated by the flowchart in Figure 2. While the flowchart is for the most part self-explanatory, some aspects of the algorithm and its design merit further discussion.

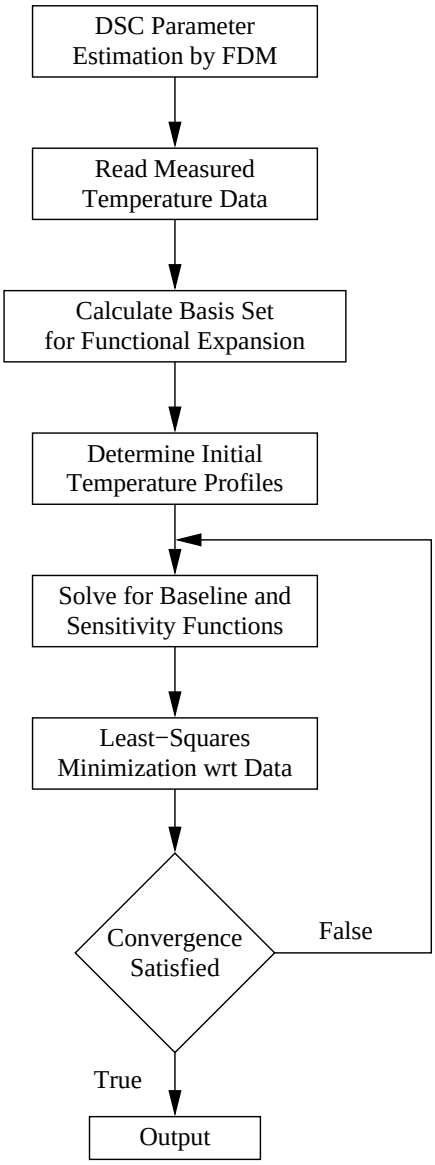

Figure 2. Basic flowchart for DSC parameter estimation computational algorithm.

The first point of interest is the basis set used in the functional expansion for the radiative contribution from the furnace wall, T_f^4. The numerical results presented in this paper have been generated utilizing Chebyshev polynomials of the first kind [2]. This particular basis set has been chosen for the initial test runs because it possesses several advantageous computational attributes and has been used previously to solve problems in many disciplines with considerable success [3–6]. It should be noted, however, that other choices exist which may yield the desired results without requiring as many expansion terms.

Another important detail of the computational algorithm is the manner in which initial temperature profiles are calculated. Because the quasilinearization scheme is based on the Newton-Raphson technique, the 'guesses' employed as established values for the first iteration can considerably influence the rate of convergence and, if physically unrealistic, the final results. Therefore, it is beneficial to begin the numerical simulation with educated estimates. For the algorithm presented here, the initial temperature profiles are determined with respect to the measured temperature data and the primary estimates for the unknown system parameters. The process involves the development of functional representations for the measured data streams and resolution of a direct problem for both the sample-side and reference-side components. This small expenditure of computational effort helps to ensure faster convergence and increased stability.

Finally, a few comments should be made regarding iterative convergence criteria. The present scheme has the capability to employ the infinity norm of either the system parameters or the sensitivity functions between iterations. While the latter convergence criteria are more rigorous, it has been found that for the numerical experiment presented the former are sufficient to obtain results consistent with the likely precision of the DSC instrument (four significant digits).

4 Numerical Results

A numerical experiment has been designed to test the proposed model and algorithm. It should be reiterated that the model and numerical implementation are preliminary and some refinement is expected before using 'real' experimental DSC data. Component masses for the theoretical two-pan heat-flux DSC are defined as $m_{sc} = 0.2558$ g, $m_{sp} = 0.1039$ g, $m_{rc} = 0.2596$ g, and $m_{rp} = 0.1059$ g. For the purpose of this investigation, all components are assumed to be made of pure platinum and possess a corresponding temperature-independent average value for specific heat capacity, $C = 0.152$ J/g-K. Using this system, a direct problem has been solved for a furnace wall temperature profile as described in Fig. 1 with $t_0 = 30$ s, $t_1 = 2115$ s, $t_2 = 4200$ s, $t_{max} = 6000$ s, $T_o = 300$ K, $T_{max} = 1516$ K, and $\mu = 0.333$ K/s (corresponding to 20 K/min). The resulting discrete temperature values for both the sample and reference plates are designated as data for the parameter estimation algorithm.

Both errorless and noisy data are used as input for the computational algorithm. Noisy data are generated in accordance to

$$T_{sp,i} = T_{sp}(t_i) + \epsilon Rand(i) T_{sp}(0), \tag{4a}$$

$$T_{rp,i} = T_{rp}(t_i) + \epsilon Rand(i) T_{rp}(0), \quad i = 1, \cdots, M, \tag{4b}$$

where $t_i = i\Delta t$, with $\Delta t = t_{max}/M$, M is the total number of data points, ϵ is the noise factor chosen from the closed interval [0,1], and $Rand(i)$ represents the i^{th} randomly drawn real number from the closed interval [-1,1].

To begin, consideration of ideal, errorless data ($\epsilon = 0$ and $M = 60001$) is used to illustrate recovery of the input parameters, K_{sp}, K_{rp}, E_{fp}, E_{fc} and the furnace wall

temperature $T_f(t)$. Converged estimations for the unknown system parameters compared with the values used to solve the direct problem are shown in Table 1. Likewise, the reconstructed temperature profiles are presented in Fig. 3. Convergence occurs when eighty terms ($R = 80$) are used in the functional expansion for T_f^4. As can be seen, the proposed model produces excellent results. It should be noted that this simulation resolves $R + 4$ parameters simultaneously.

Parameter	Exact	Estimated
K_{sp}	2.500E-01	2.498E-01
K_{rp}	2.700E-01	2.696E-01
E_{fc}	1.000E-03	1.001E-03
E_{fp}	2.500E-04	2.490E-04

Table 1. Comparison of exact and numerically estimated values for the DSC system parameters. Eighty terms have been used in the functional expansion ($R = 80$).

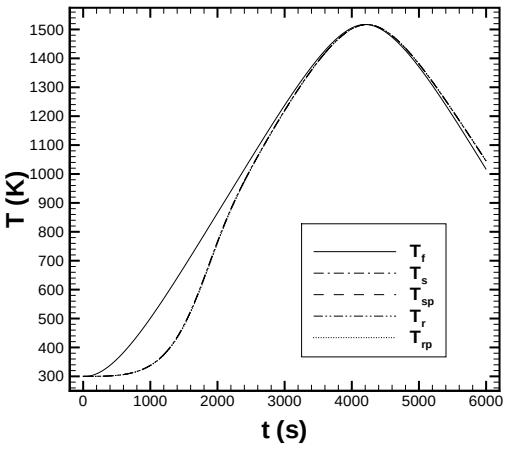

Figure 3. Temperature profiles for the four DSC components and the reconstructed furnace wall temperature generated by the parameter estimation algorithm ($R = 80$).

Figure 4 presents the trend toward convergence for the numerical estimations of the parameters as the number of expansion coefficients in the reconstruction of $T_f(t)$ is increased. Figure 4(a) displays results for the conduction-related parameters while Fig. 4(b) presents the radiation-related parameters. These figures indicate that accurate and stable reconstruction of the thermophysical parameters are obtained as the number of terms R in the expansion for $T_f(t)$ is increased. For the chosen basis set, approximately

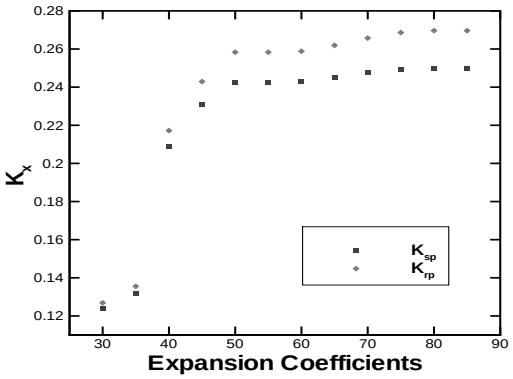

(a) Convergence for conduction-related parameters K_{sp} and K_{rp}.

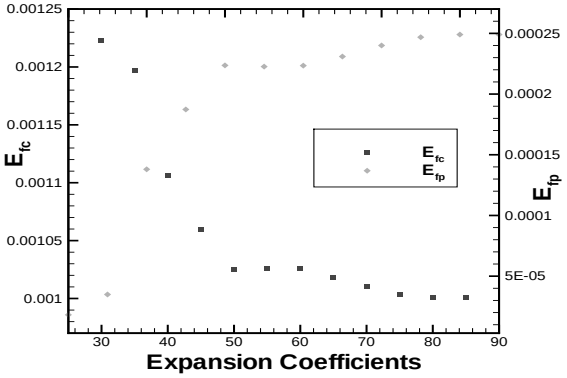

(b) Convergence for radiation-related parameters E_{fc} and E_{fp}.

Figure 4: Numerical convergence of unknown system parameters with respect to the number of expansion terms used to reconstruct the furnace wall temperature.

80 terms of the series are required. As mentioned earlier, a change of basis to one which is better tailored to the profile of $T_f^4(t)$ can substantially reduce the number of coefficients required in reconstructing the furnace wall temperature.

Figures 5a-c display comparisons between the direct and reconstructed inverse predictions for (a) $T_f(t)$, (b) $T_s(t)$, and (c) $T_r(t)$. It is clear that the direct results are recovered by the proposed method. Figures 6a-c illustrate convergence results as R is increased for (a) $T_f(t)$, (b) $T_s(t)$, and (c) $T_r(t)$. Again, it appears that $R = 80$ is required for establishing an accurate prediction.

Figures 7–15 present the baseline and sensitivity functions pertaining to the system parameters for the four DSC components. As expected, the baseline functions shown in Fig. 7 closely follow the shape of their respec-

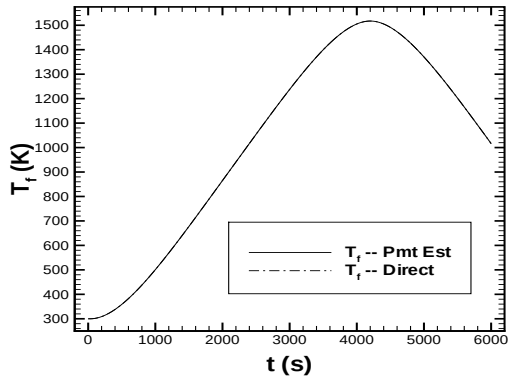

(a) T_f reconstructed by the parameter estimation code vs. T_f used in the direct code.

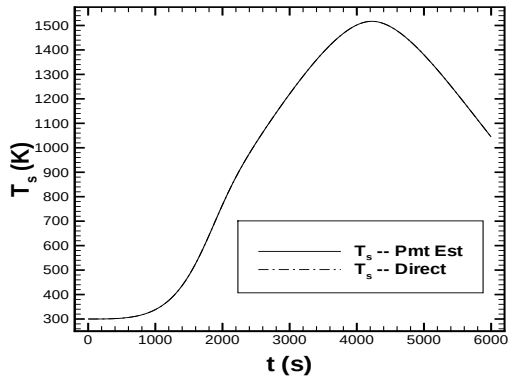

(b) T_s reconstructed by the parameter estimation code vs. T_s generated by the direct code.

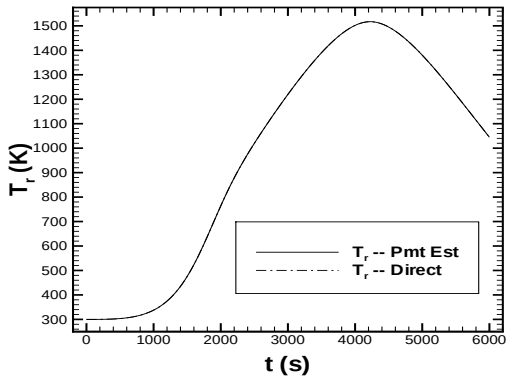

(c) T_r reconstructed by the parameter estimation code vs. T_r generated by the direct code.

Figure 5: Comparison of the direct solution temperature profiles with those reconstructed by the parameter estimation algorithm ($R = 80$).

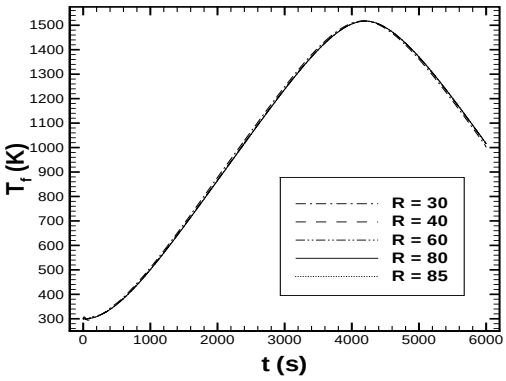

(a) Convergence for reconstructed T_f with respect to number of expansion terms.

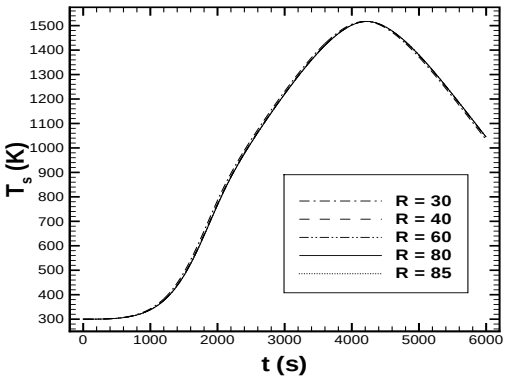

(b) Convergence for reconstructed T_s with respect to number of expansion terms.

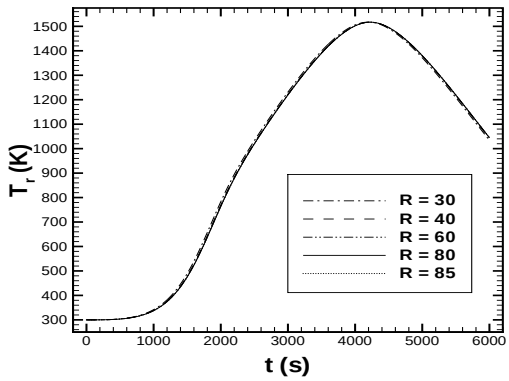

(c) Convergence for reconstructed T_r with respect to number of expansion terms.

Figure 6: Convergence as a function of the number of expansion terms, R, for the reconstructed temperature functions of selected components.

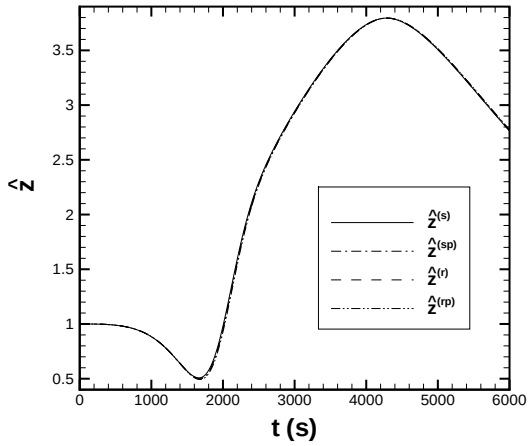

Figure 7: Converged baseline functions, $\hat{z}^{(s)}$, $\hat{z}^{(sp)}$, $\hat{z}^{(r)}$, $\hat{z}^{(rp)}$, for the four DSC components.

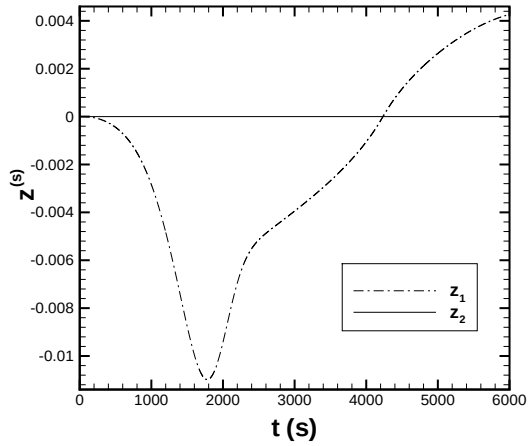

Figure 8: Sensitivity functions corresponding to K_{sp} and K_{rp} for the sample component.

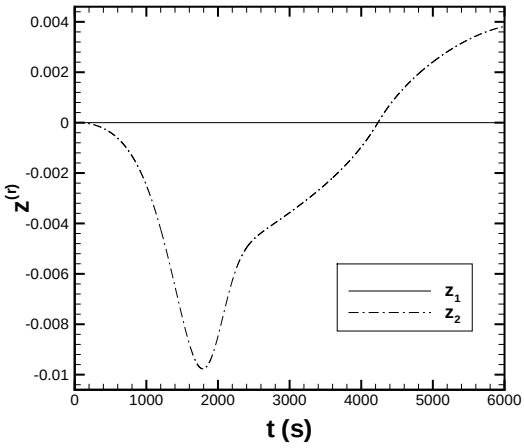

Figure 9: Sensitivity functions corresponding to K_{sp} and K_{rp} for the reference component.

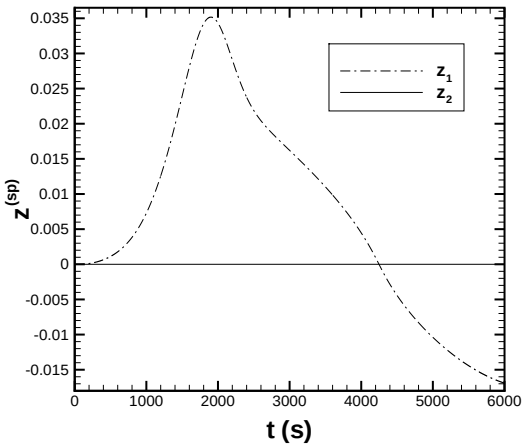

Figure 10: Sensitivity functions corresponding to K_{sp} and K_{rp} for the sample plate.

tive component temperature profiles and so indicate their leading influence in the reconstruction of the temperature functions. More interesting, however, is the behavior of the sensitivity functions seen in Figs. 8–11. Here, the lack of cross communication mentioned earlier is clearly demonstrated by the fact that $z_2(t)$, which corresponds to conduction between the reference plate and container, is uniformly zero for the sample-side components and $z_1(t)$, which corresponds to conduction between the sample plate and container, is uniformly zero for the reference-side components. This behavior underscores the need for two concurrent data streams in the model since information pertaining to all the parameters must be present in the data used for minimization.

Finally, to illustrate a realistic situation, some random error is introduced into the data streams for $\{T_{sp,i}\}_{i=1}^{M}$ and $\{T_{rp,i}\}_{i=1}^{M}$. The value of ϵ has been chosen such that the maximum error is ± 0.25 K. The reconstructed furnace wall

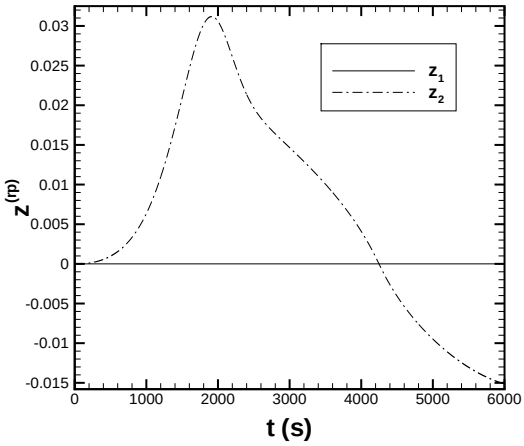

Figure 11: Sensitivity functions corresponding to K_{sp} and K_{rp} for the reference plate.

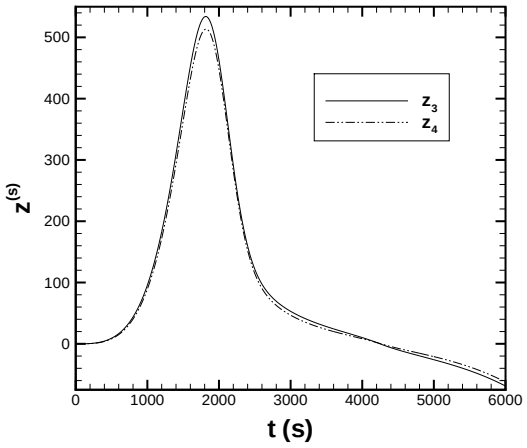

Figure 12: Sensitivity functions corresponding to E_{fc} and E_{fp} for the sample component.

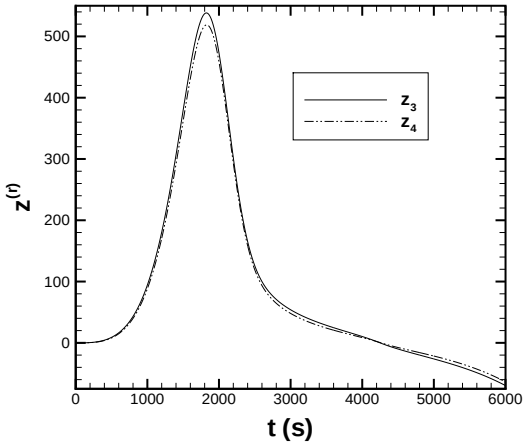

Figure 13: Sensitivity functions corresponding to E_{fc} and E_{fp} for the reference component.

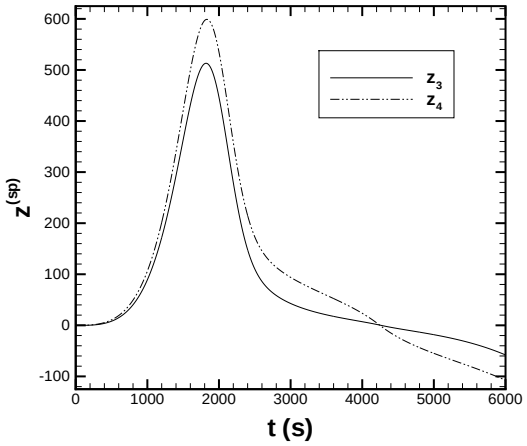

Figure 14: Sensitivity functions corresponding to E_{fc} and E_{fp} for the sample plate.

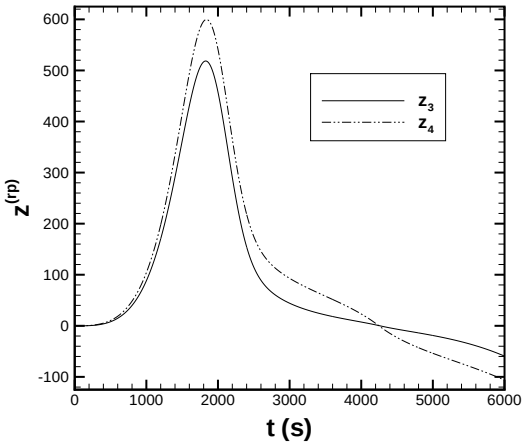

Figure 15: Sensitivity functions corresponding to E_{fc} and E_{fp} for the reference plate.

temperature profile, along with its counterpart used to drive the direct problem, are shown in Fig. 16. These profiles are graphically equivalent and indicate that the algorithm remains stable in the presence of noise. Similarly, converged estimations of the system parameters are compared with the exact values in Table 2. As expected, noise in the data has an affect on accuracy, but the results are still quite good and fall within acceptable tolerances. It can be envisioned that parameter recovery is an area where time collocation, which minimizes the effects of local errors by taking the entire domain into account, will provide substantial improvement over traditional time-marching schemes.

Parameter	Exact	Estimated
K_{sp}	2.500E-01	2.506E-01
K_{rp}	2.700E-01	2.760E-01
E_{fc}	1.000E-03	9.754E-04
E_{fp}	2.500E-04	2.744E-04

Table 2. Comparison of exact and numerically estimated values for the DSC system parameters with error introduced into the data. 90 terms have been used in the functional expansion ($R = 90$).

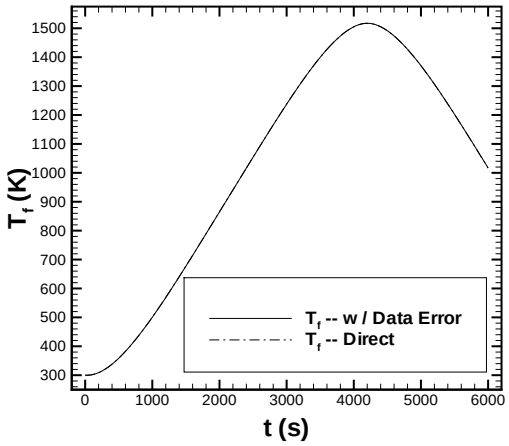

Figure 16: Reconstructed T_f generated by the parameter estimation algorithm with error introduced into the data ($R = 90$) compared with T_f used in the direct code.

5 Conclusions

This paper illustrates the effectiveness of the proposed inverse algorithm presented in [1]. The results are encouraging and refinement of the approach is presently underway. Several improvements can be identified including: (1) changing the basis set used in representing $T_f(t)$ in order to reduce the parameter set size associated with the expansion coefficients for $T_f(t)$; and (2) using a time-collocation approach to substantially reduce the memory and CPU requirements for solving the system of initial-value problems in the sensitivity variables. Item 2 permits alignment independence between the computational grid and experimental time domain without requiring any intermediate interpolation or numerical grid/experimental data point coexistence. This produces a substantial reduction in programming effort in the entire minimization process and in the updating procedure associated with the quasilinearization method. Time collocation also assists in stabilizing inverse predictions because of the whole-domain accountability.

Model refinement is also being pursued. The present set of papers demonstrates a numerical approach that warrants further consideration and implementation refinements. The goal of the research effort under consideration by the authors involves modeling real-world DSC events.

Acknowledgments

This work was supported under a DOE grant provided to the University of Tennessee under the Industrial Materials for the Future Program (DE-FC07-01ID14249).

References

[1] G. E. Osborne, J. I. Frankel, and A. Sabau. A new parameter estimation method for DSC thermodynamic property evaluation – part I: analytic development. In *Twenty-Second IASTED International Conference on Modelling, Identification, and Control*, Innsbruck, Austria, February 10–13 2003.

[2] D. Gottlieb and S. A. Orszag. *Numerical Analysis of Spectral Methods*. SIAM, Philadelphia, PA, 1977.

[3] J. I. Frankel. Cumulative variable formulation for transient conductive and radiative transport in participating media. *Journal of Thermophysical Heat Transfer*, 9(2):210–218, 1995.

[4] J. I. Frankel and G. E. Osborne. A new time treatment for solving partial-integro differential equations of radiative transport. *IMA Journal of Numerical Analysis*, 19:91–103, 1999.

[5] A. C. Kaya and F. Erdogen. On the solution of integral equations with strongly singular kernels. *Quarterly of Applied Mathematics*, 45(1):105–122, 1987.

[6] S. A. Orszag. Accurate solution of the Orr-Sommerfeld stability equation. *Journal of Fluid Mechanics*, 50(4):689–703, 1971.

[7] M. Abramowitz and I. A. Stegun. *Handbook of Mathematical Functions*. Dover, New York, 1972.